Contemporary Mathematics
http://ojs.wiserpub.com/index.php/CM/

UNIVERSAL WISER PUBLISHER

Research Article

A Mathematical Approach Towards Random Road Profile Generation Based on Chaotic Signals of Chua's Circuit

Sina Milani[1], Aidin Momtaz[2], Sarah Amini[3], Kasra Amini[4*], Shekoufeh Sadeghi[3], Ehsan Qoreishi[2], Sanaz Haddadian[5]

[1]School of Engineering, RMIT University, Melbourne, Australia
[2]Department of Physics, Isfahan University of Technology, Isfahan, Iran
[3]Department of Computer Engineering, K. N. Toosi University of Technology, Tehran, Iran
[4]FLOW and Fluid Physics Laboratory, Department of Engineering Mechanics, KTH Royal Institute of Technology, Stockholm, Sweden
[5]System and Circuit Technology Group, Heinz Nixdorf Institute, University of Paderborn, Paderborn, Germany
E-mail: kasraa@kth.se

Received: 13 September 2021; **Revised:** 20 December 2021; **Accepted:** 07 January 2022

Abstract: In response to application demands in vehicle dynamics and control, traffic engineering, urban planning, and logistics, the generation of an adequate artificial road profile in terms of the diversity of geometric scenarios has been addressed in the current manuscript. The underlying mathematical principles for generating a geometrically comprehensive, yet logically meaningful, 3D road profile have been taken from high and unbiased sweeping factors of random number sequences over their domain of interest. And to generate such random number sequences, the mathematically manipulated output signal of a well-established chaotic system has been utilized, namely that of the Chua's circuit. Having defined the target road profile mathematically with all its geometrical complexities, a suitable scheme derived from the mentioned chaotic signal has been used to generate the required random number sequences as defining parameters of the road profile. The scheme has been otherwise tested and proven to show the demanded level of randomness in literature. Several attempts have been made to create a diverse range of road profiles, considering the constraints imposed by vehicle dynamics. To generate the road geometries, the limitations imposed by the vehicle's motion, such as the limitations on corresponding curvatures, slopes, and banking angles are negotiated, in terms of vehicle dynamics and available tire-road friction forces, by evaluating how close a vehicle will be to its tire force capacity limits as it travels on sections of the generated road.

***Keywords*:** road curvature, road profile, 3D curve generation, chaos theory, Chua's circuit, random number sequence

Nomenclature

Latin Letters

B_P	Breakpoint of current	[v]
C	Capacitor	[F]
G	Slope of Chua's diode	[A/v]

DOI: https://doi.org/10.37256/cm.3120221151

i	Current	[A]
L	Self-inductance	[L]
R	Resistance	[Ω]
V	Voltage	[v]
x	Dimensionless state variable	[-]
y	Dimensionless state variable	[-]
z	Dimensionless state variable	[-]
$V(x_v, y_v, z_v)$	Vehicle body-fixed coordinate frame	[m]
$R(x_r, y_r, z_r)$	Road coordinate frame	[m]
$G(X, Y, Z)$	Global coordinate frame	[m]
u_i	Unit vectors	[m]
r_0	Last position vector of center of curvature	[m]
r	New position vector of center of curvature	[m]
$r_{A,B}$	Position vector from A to B	[m]
C_{ijk}	Center of curvature of the arc ijk	[-]
$R_{u,\alpha}$	Rotation about u with angle α transformation matrix	[-]
g	Gravitational acceleration	[m/s^2]
$a_{x,y,z}$	Acceleration along x, y, z axes	[m/s^2]
a_c	Centripetal acceleration	[m/s^2]
v	Vehicle translational velocity	[m/s]
$F_{x,y,z}$	Forces along x, y, z axes	[N]
m	Vehicle mass	[kg]
$\hat{i}_F$, $\hat{j}_F$, $\hat{k}_F$	Unit vectors of frame F	[m]

Greek Letters

α	Dimensionless parameter	[-]
β	Dimensionless parameter	[-]
ψ	Road waypoints' angular increment	[rad]
θ	Center of curvature angular position	[rad]
ϕ_{ij}	Vertical road slope between points i, j	[rad]
ρ	Radius of curvature	[m]
μ	Friction coefficient	[-]
γ	Road bank angle	[rad]
ζ	Elevation angle of center of curvature in vehicle frame	[rad]
τ	Independent road variable	[-]

Abbreviations

RNG	Random Number Generator
TRNG	True Random Number Generator
PRNG	Pseudo Random Number Generator
LFSR	Linear Feedback Shift Registers
TFU	Tire Friction Usage
CoC	Center of Curvature
FPGA	Field-Programmable Gate Array
NIST	National Institute for Standards and Technology
GIS	Geographic Information System
LSODA	Livermore Solver for Ordinary Differential Equations

Subscripts

1	Numbering index
2	Numbering index
a	Inner slope
b	Outer slope
L	Inductor
R	Resistance

1. Introduction

Considering the ever-increasing trend for creating simulation conditions as close to the actual physical setting as technologically possible, generation of road profiles and systems are of great importance in traffic flow simulation, vehicle dynamics and control studies as well as simulations of logistics. As a road profile diverges from a 1D curved function in 2D or 3D space and approaches its actual conditions, a more comprehensively diverse ansatz should be implemented to define it for the specific application in question.

Artificial random road geometries that resemble real roads are of great significance in certain simulation studies, especially when the information regarding real roads is unavailable or a system is to be evaluated or designed based on a generic road profile representing a wide range of real situations, rather than being limited to a particular already-existing road. For instance, a randomly auto-generated road geometry may be used in training a neural network for a specific task such as vehicle directional control or energy management. More to the point, a randomly generated road may be used to evaluate a certain developed vehicle control system to assess its efficacy in any potential scenario. Although manual road generation could be done using computer software and user inputs, a manual process will not guarantee the randomness and diversity of the resulting road geometries, which is crucial in certain applications such as training artificial intelligence systems.

With the above considerations in mind, such details of the mathematical approach and algorithms towards defining a functionally adequate road geometry for the purposes of vehicle dynamics and traffic flow simulations using a previously established random number generator is to be addressed in the current manuscript.

1.1 *Literature survey-chaos theory*

A chaotic system, similar to any dynamical system, consists of deterministic rather than underlying probabilistic rules, which every future state of the system must follow. In addition, such systems must behave in specific conditions known to the experts in the field, to be called chaotic. First, they are unstable with respect to slight modifications. This sensitivity to the initial conditions causes them to evolve into a considerably different state when a slight perturbation is applied [1]. This particular fact makes a long-term prediction mostly impossible, and the future state could be known only to a finite degree of precision. Also, nonlinearity and aperiodic behavior should be observed in a signal for it to completely fit into the chaotic category [2].

The Analytical studies of planetary motion with a geometric approach by Poincare (1890) led to the development of nonlinear dynamics and chaos [3]. After all the investigations on nonlinear dynamics, the chaos theory was born in Lorenz's identification of ordinary nonlinear differential equations designed to represent dissipative hydrodynamic flows [4]. Formerly, Lorenz's achievements and his interpretation of chaos were reflected in applied engineering [5], economics and biological studies.

Pseudo Random Number Generators (PRNGs), such as Linear Feedback Shift Registers (LFSRs) and software-based random number generators are widely used in deterministic random number generation systems. The random numbers, however, are repeatable. True Random Number Generators (TRNGs) rely on physical sources of randomness to ensure unpredictability. Thermal noises, Magnetic Tunnel Junctions, chaotic phenomena, free-running oscillators, photo cameras are example sources of TRNGs [6-8].

Random sequences generated by chaotic systems in electronic circuits are considered as an excellent source for cryptographic applications due to their unpredictable nature [9]. In order to derive sophisticated PRNGs from the

datasets extracted from a classical Chua's system, 8 mathematical schemes were designed with the outputs of binary sequences. Then, NIST statistical tests were applied to evaluate the randomness level of each sequence. Three of which were chosen as standard PRNGs that satisfied the mandatory criteria. Moreover, many attempts have been established to evaluate the validity of random outputs extracted from chaotic signals, from which certified random number generators are selected in the current manuscript [10-11].

The idea of deriving RNGs from chaotic systems has been popularized by numerous research attempts, addressing the legitimacy of this approach. Regarding cryptographic applications, it has been demonstrated in [12], that chaotic systems could be successfully applied as building blocks for random number generators. A configurable PRNG template that is parametrized using a chaotic map is presented in the cited research. In earlier research by [13], two algorithms were designed to produce pseudo random number sequences from a single generalized Lorenz system, which were subsequently evaluated with the NIST statistical tests. In addition, since numerous possible variations for analyzing the output signal of a chaotic system exist, the feasible options for schemes to derive PRNGs and TRNGs differ widely. In [14], four different chaotic attractors have been generated from Lorenz and Lü chaotic systems. Furthermore, the PRNG is set to a new reconfiguration embedded in an FPGA cascaded encryption processor; a relatively commonplace approach to exploit reconfiguration features [15-16]. On the other hand, TRNG circuits play a critical role in hardware security. TRNGs based on dual oscillator architecture and a chaotic ring oscillator have been proposed in [17-18], respectively.

1.2 *Literature survey-road application*

The random nature of the road geometry has been studied for many years, with a wide majority of studies being conducted on the road surface roughness, aiming at modelling the road surfaces stochastically, to be used in vehicle ride comfort as well as Noise-Vibration-Harshness studies [19-27], where some of the earliest works in this regard could be attributed to [28-30].

Besides the road surface roughness modeling, a number of studies have focused on the detection of real road data, including the road boundaries and curvature profile based on the information gathered through vehicles' cameras, and performing image processing, mainly for the purpose of identifying the surrounding environment in autonomous and semi-autonomous vehicles [31-35]. Furthermore, the conversion of GIS data from real roads into three dimensional geometries has been conducted in [36-38].

Huang et al. [39] constructed an artificial road geometry based on real road data to provide a basis for optimizing a vehicle powertrain control system to minimize fuel consumption.

Jo and Sunwoo [40] developed a method to construct a model of real road geometries by means of a probe vehicle and using its GPS and inertial measurements, to be used for path detection of autonomous vehicles, when such data are temporarily unavailable.

Mao and Li [41] developed a method to automatically generate road segments based on the arbitrary user inputs to construct road curves using cubic Hermite interpolation algorithm.

Although the above methods were introduced to develop road geometry information, a majority of them are focused on modeling already-existing roads or are incapable of producing randomly generated roads automatically.

Zeng and Wang [42] used stochastic road grade information for the stochastic dynamic programming optimization within their model predictive controller to optimize the energy efficiency of hybrid electric vehicles. However, the model does not include road curvatures and does not possess three-dimensional features.

Khayyam [43] introduced an artificial road modeling algorithm using stochastic data to mimic real three-dimensional road geometries, mainly for the purpose of being used in the energy management of hybrid electric vehicles. The model is capable of generating slopes, bends, and wind direction based on proper distribution functions. Although the model is efficient in providing random scenarios for vehicle energy management studies and longitudinal dynamics, the model is based on independent generation of this information, which may not necessarily represent a certain curve in 3D space, therefore may not be sufficient for lateral vehicle dynamics considerations.

Johannesson et al. [44] developed a stochastic road topology modeling based on the Gaussian AR(1) process, which is able to generate realistic artificial road slope information. Based on this methodology, Odrigo et al. [45] introduced a road generation algorithm capable of generating independent slope, curvature, and roughness information based on the Volvo Global Transport Application. Although three-dimensional road profiles are obtained, each feature (i.e.

slope, curvature, roughness) is generated independently, and the curvature construction is based on connecting straight sections to constant curvature sections via transition curves, which may limit the diversity in the resulting road sections.

Focusing on the longitudinal vehicle motion, Pettersson [46] developed the required information for the individual road data in a mid-level description of the road, based on the methods described above, which rely on the stochastic curvature, topographic, road roughness, or even the traffic signage data to develop operating cycles and speed profiles for vehicle emission and energy management studies; however, the lateral vehicle dynamics and three-dimensional characteristics of the road have not been addressed.

Torabi [47] used Bezier curves to model the elevation along the road via control points from real measurement data. This information is used to develop a speed profile optimization scheme with the objective of energy consumption of vehicles; therefore, the main focus of the work is on longitudinal vehicle motion and energy balance.

Although the above studies developed road identification, reconstruction, and auto-generation algorithms, they have mainly focused on vehicle vibrations and energy management studies, while no particular attention has been made to lateral vehicle dynamics, which is key in dealing with autonomous driving systems and vehicle stability analysis. This may also be observed by usually ignoring the banking of the road segments in corners. As a major research gap in the area of random road generation algorithms based on mathematical geometry and linear algebra, a comprehensive three-dimensional road geometry generation algorithm based on regulated random data is needed in order to integrate the curvature, slope, and banking information into a realistic three-dimensional road profile to be used in evaluation and training procedures using simulated scenarios. In addition to that, the limits of vehicle traction forces and consideration of feasibility of the generated roads in terms of vehicle dynamics have not been previously established.

Therefore, the goal and scientific contribution of this study is to develop and introduce a framework for generation of realistic and controllable random road geometries with focus on three-dimensional spatial curves and required considerations of the road design, including curvature continuity, slope limitations, and road banking, in order to propose a more inclusive solution to random road modeling that can be used in both vehicle energy management studies and vehicle lateral control/stability investigations. Special attention is given to making sure the resulting geometries satisfy the predefined necessary conditions (i.e. design limits) and the anticipated high diversity of the output road geometries is achieved. To construct the intended road geometries in a creative and novel way, and to ensure the required curvature continuity, the manipulated center of curvature of the road is directly used to draw different segments of the road in small increments.

To the best of the authors' knowledge, there is currently no published work that is able to generate all this information regarding the road geometry with regulated random numbers, while considering the physical limitations and feasibility of the road geometry for vehicle dynamics; therefore, the presented approach marks a novel algorithm development for studies requiring random yet realistic and feasible environment for vehicle dynamics simulations, training of AI systems, or control system validation. From a scientific point of view, the proposed approach contributes to the existing literature by utilizing a numerical process and linear algebra to develop a physically meaningful geometry, representing a real-life situation, which facilitates the development and evaluation of smart control systems, by providing a realistic diverse virtual simulation environment.

1.3 *Paper summary*

The paper opens with insights on the mathematical definition of a road and its geometric manifestations. This includes the model of the road and concerns regarding its limitations in terms of continuous variation of its geometric parameters. In the section on methodology, first, the source of the random number sequences, namely the chaotic output signal of Chua's circuit, is discussed. Then, the specifics of the algorithm designed to generate the road profile based on the required inputs from specially manipulated sets of random number sequences are introduced, leading to the hypothetical results and evaluation criteria for the resulting road profiles. Finally, the paper is to be closed with extensive discussions on the road profiles as the actual results of the work.

2. Mathematical definition of the road

2.1 *Road modeling*

In order to completely define a three-dimensional road profile, a number of parameters need to be known at every point on the trajectory. These points on the road profile may be defined using an independent parameter τ which varies between zero and one as the object moves from the initial point towards the destination (i.e. the end point of the road). Each value of $0 \leq \tau \leq 1$ corresponds to a specific point on the road as a three-dimensional curve in space. The curve could be viewed as the centerline of the road on which a vehicle is supposed to be traveling. Such a representation requires three coordinates to be known/determined at each value of the independent parameter τ, namely those of the $x(\tau)$, $y(\tau)$, and $z(\tau)$.

For a 3D curve, the osculating plane is defined as the plane passing through three differentially adjacent points on the curve (see Figure 1). The osculating plane contains the circle created using these three points, and consequently, the center of curvature of the road profile at that specific vicinity, which is coincident with the center of the aforementioned circle. This circle may be called the "osculating circle".

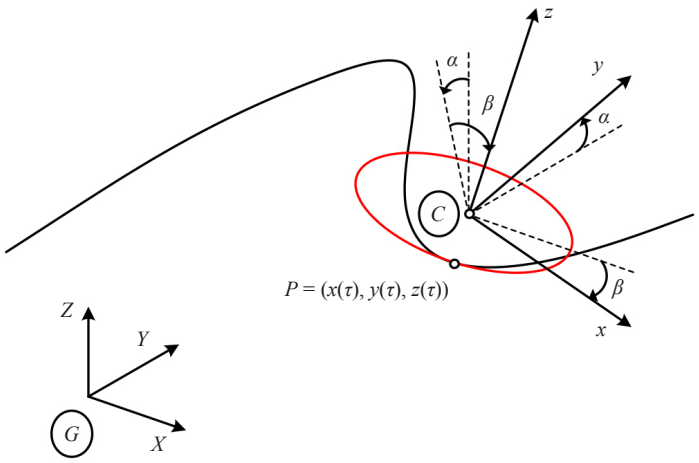

Figure 1. Road as a 3D curve with the osculating circle and the center of curvature

To employ the effect of the road bank angle, an additional parameter $\gamma(\tau)$ is also required to represent the degree of tilting at each point on the road, with respect to a reference horizontal plane. Note that the bank angle information is not included in the osculating circle in Figure 1, as a curve does not include any information on the orientation of the road surface itself, but it only provides the coordinates of the road's centerline. The degree of tilting represents the lateral slope of the road surface, which will be constructed using the curve in Figure 1, measured about the tangent line to the road. In other words, there are a total of four degrees of freedom in the mathematical modeling of the road profile. It is worth mentioning that, in this paper, we assume the road surface to be smooth and the road roughness modeling for vehicle ride comfort studies to be beyond the scope of this work.

Therefore, a complete mathematical representation of a road profile contains an independent parameter τ and four parameters as functions of τ, namely $x(\tau)$, $y(\tau)$, $z(\tau)$, $\gamma(\tau)$, which need to be defined with a certain resolution of $0 \leq \tau \leq 1$ along the road and be presented/stored as a numerical table.

There are limitations on how sharp the corners of the road could be in order for a passenger vehicle to track the road without experiencing loss of tire-road friction. These limits may be translated and defined in the vehicle's coordinate frame V, which is attached to the vehicle's mass center and rotates with it as a rigid body, shown in Figure 2, and the road-fitted coordinate frame R. These limits are discussed in the methodology section.

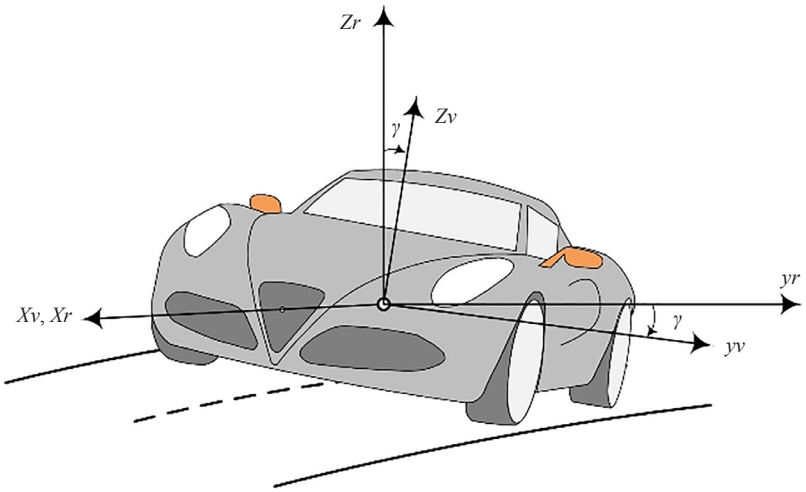

Figure 2. Vehicle coordinate frame

3. Methodology

3.1 *Research strategy*

The current manuscript revolves around the mathematical ansatz in generating a road profile with meaningful geometric configuration from a vehicle dynamics point of view.

The chaotic output signal of the classical Chua's circuit is manipulated mathematically to provide useable, functionally adequate random number sequences. These sequences are then inserted into the methodical generation algorithms introduced in the current section, for numerical generation of the road profile coordinates, local radii of curvature and its planar orientation. The resulting road profiles are either the direct outcome of having the two mentioned parameters being the random number sequences in each step of the road, the product of their first derivative being the random sequence or that of their second derivative being the level at which the randomness is introduced to the system.

The final section of the paper is, then, dedicated to the presentation of the resulting road profiles, while being subjected to a vehicle dynamics analysis to validate the preliminary justifications of the profiles.

3.2 *Chua's circuit*

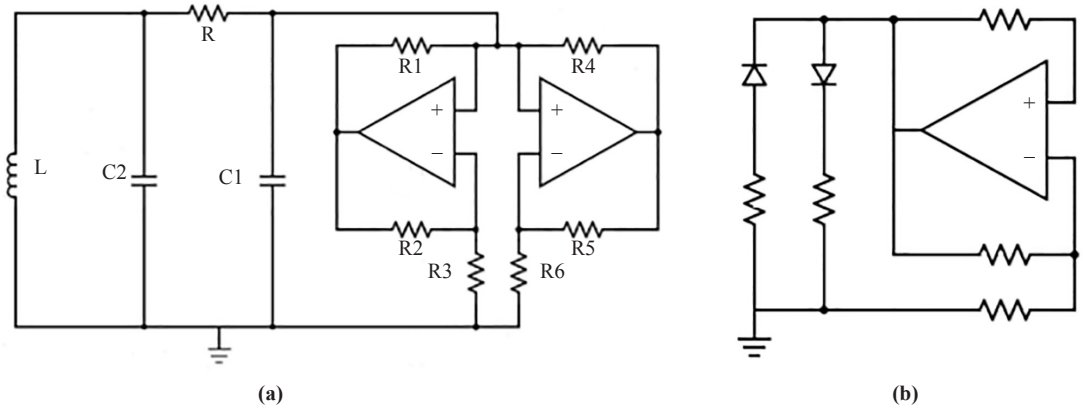

Figure 3. Chua's circuit a) amplifier base configuration b) diode base configuration

Chua's circuit plays an important role in the field of chaos and nonlinear dynamics. The simplest form of Chua's circuit could be manufactured using both linear and nonlinear elements. The linear elements include an inductor, a resistor, and two capacitors. The nonlinear section mainly consists of Chua's diode which was assembled with operational amplifiers for the purpose of current research [48]. However, another implementation of the mentioned element using diodes has been frequently applied in Chua's circuit. Both of the mentioned configurations can be observed in Figure 3.

Chua's circuit nonlinear differential equations can be formulated as below [49];

$$C_1 \frac{dV_R}{dt} = \frac{V_{C_2} - V_R}{R} - f(V_R), \tag{1}$$

$$C_2 \frac{dV_{C_2}}{dt} = i_L - \frac{V_{C_2} - V_R}{R}, \tag{2}$$

$$L \frac{di_L}{dt} = -V_{C_2}, \tag{3}$$

where V_{C_1}, V_{C_2} and i_L represent the voltages of the C_1 and C_2 capacitors and the current of the inductor L, respectively, and $f(V_R)$ is a nonlinear function defined as;

$$f(V_R) = G_b V_R + \frac{(G_a - G_b) \times \{|V_R + B_P| - |V_R - B_P|\}}{2} \tag{4}$$

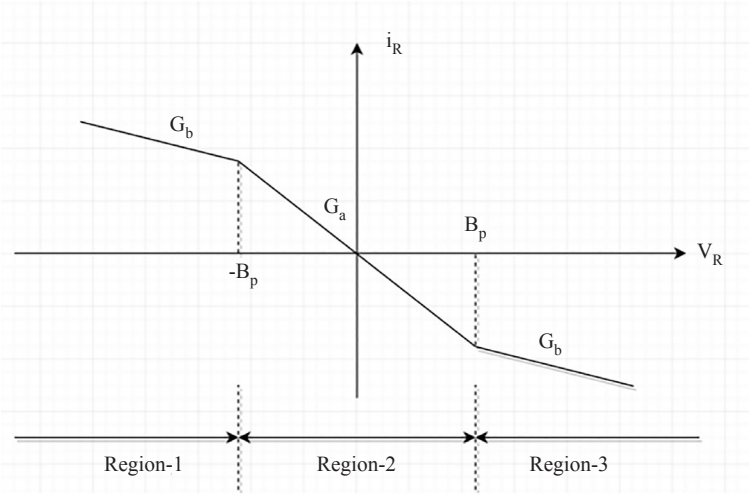

Figure 4. Current vs voltage alteration of Chua's diode graph [10]

$$G_b V_R + (G_b - G_a) B_P, \; V_R < -B_P \tag{5}$$

$$G_a V_R, \; -B_P \le V_R \le B_P \tag{6}$$

$$G_b V_R + (G_a - G_b) B_P, \; V_R > B_P \tag{7}$$

$f(V_R)$ represents the nonlinear part of the equations in which G_a and G_b are considered as the inner and outer slopes of Chua's diode, respectively, and $+B_P$ are the breakpoints in i_R (Figure 4).

Having dimensionless equations will make them easier to use. This is accomplished by defining variables as $x = \frac{V_{C_1}}{B_P}$, $y = \frac{V_{C_2}}{B_P}$, and $z = (\frac{R}{B_P})$. i_L, and parameters like $\alpha = \frac{C_2}{C_1}$ and $\beta = \frac{R^2 C_2}{L}$ without physical dimensions [48].

$$dx / dt = \alpha(y - x - f(x)) \tag{8}$$

$$dy / dt = x - y + z \tag{9}$$

$$dz / dt = -\beta y \tag{10}$$

Since Chua's circuits are classified as chaotic systems with high dependency on initial values, another way to demonstrate Chua's circuit's chaotic stability is by analyzing its strange attractors. Alteration of the parameter β when the other parameters are fixed can finally result in the occurrence of the chaotic behavior reflected in the so-called double scrolls (Figure 5).

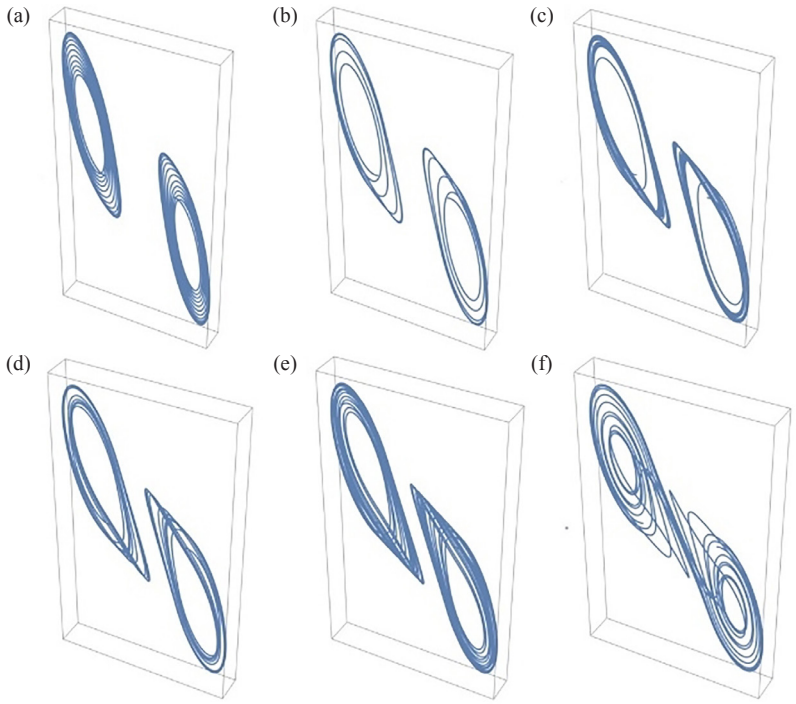

Figure 5. Fixed parameters are $\alpha = 15.5$, $G_a = \frac{8}{7}$, and $G_b = \frac{5}{7}$. The attracting set starts to variate as parameter β changes. a) $\beta = 50$, two periodic orbits. b) $\beta = 40$, the orbits have "period-doubled". c) $\beta = 35$, another doubling of the period. d) $\beta = 34$, a pair of chaotic attracting orbits. e) $\beta = 33$, the chaotic attractors expand and move towards one another. f) $\beta = 28$, a "double scroll" chaotic attractor [11]

3.3 *Road generation algorithm*

Based on the mathematical road modeling remarks in section 2, a systematic methodology is described here, which enables the generation of such a road profile considering the constraints imposed by the vehicle dynamics on the

feasibility of the road, in terms of the friction forces between the tires of a vehicle and the ground.

3.3.1 *Generating the road centerline*

The concept of the osculating circle may be used to draw (generate) a parametric 3D curve step by step through a controlled process, i.e. a controlled movement/orientation of the osculating circle. In this case, the osculating circle may also be called a "drawing circle", which acts as a tool by which a parametric 3D curve could be created.

To come up with the coordinates of the parametric curve as $x(\tau)$, $y(\tau)$ and $z(\tau)$, we would first need to fix two initial points, that would serve as the reference. Next, the drawing circle needs to be configured for the creation of the third point. The drawing circle may be defined generally using three variables, defining its orientation and radius. Two angles $\alpha(\tau)$ and $\beta(\tau)$ are required to define the orientation of the drawing circle in the 3D space, namely the local roll and pitch rotations. Note that the yaw rotation does not add any information to the orientation of the circle, naturally. We may take the order of global rotations as α about the X axis and then β about the Y axis. This rotation is schematically shown for a sample point on the curve in Figure 1. A rotation matrix may be defined to relate the local coordinate frame C attached to the drawing circle, and the global frame G attached to the ground, using the rotation sequence [50];

$$
{}^{C}R_{G} = R_{y,\beta}R_{x,\alpha} = \begin{bmatrix} \cos\beta & 0 & -\sin\beta \\ 0 & 1 & 0 \\ \sin\beta & 0 & \cos\beta \end{bmatrix}\begin{bmatrix} 1 & 0 & 0 \\ 0 & \cos\alpha & \sin\alpha \\ 0 & -\sin\alpha & \cos\alpha \end{bmatrix}
$$

$$
= \begin{bmatrix} \cos\beta & \sin\alpha\sin\beta & -\cos\alpha\sin\beta \\ 0 & \cos\alpha & \sin\alpha \\ \sin\beta & -\sin\alpha\cos\beta & \cos\alpha\cos\beta \end{bmatrix}. \tag{11}
$$

Since the rotation matrices are orthogonal, the inverse transformation from frame C to G is obtained as;

$$
{}^{G}R_{C} = {}^{C}R_{G}{}^{-1} = {}^{C}R_{G}{}^{T}. \tag{12}
$$

The third parameter required to completely define the drawing circle is its radius $\rho(\tau)$, which needs to be defined independently.

Although (11) formally relates the orientation of the osculating plane with respect to the global frame in a general case, based on the first assumed pair of road coordinates, we may not be free to choose any combination of α and β for the drawing circle; therefore, an alternative approach in defining the drawing circle would be to directly use the first pair of points to find the center of the drawing circle associated with them to ensure all geometrical constraints are automatically satisfied. Figure 6 demonstrates the loci of the potential curvature center associated with points 1 and 2 denoted by C_{123} with the dotted circle. The potential curvature center is located at the radius $\rho(\tau)$, which is a separate input to the algorithm. Next, an angle $\theta(\tau)$ is needed to fix the location of C_{123} on this circle. Note that the angle $\theta(\tau)$ is measured with reference to the previous curvature center C_{012} which is assumed to be in a certain location consistent with the initial points 1 and 2. For this purpose, the vector $\boldsymbol{r_0}$ is defined as;

$$
\boldsymbol{r_0} = \rho\frac{\boldsymbol{r}_{1,C_{012}} \times \boldsymbol{r}_{1,2}}{|\boldsymbol{r}_{1,C_{012}} \times \boldsymbol{r}_{1,2}|}. \tag{13}
$$

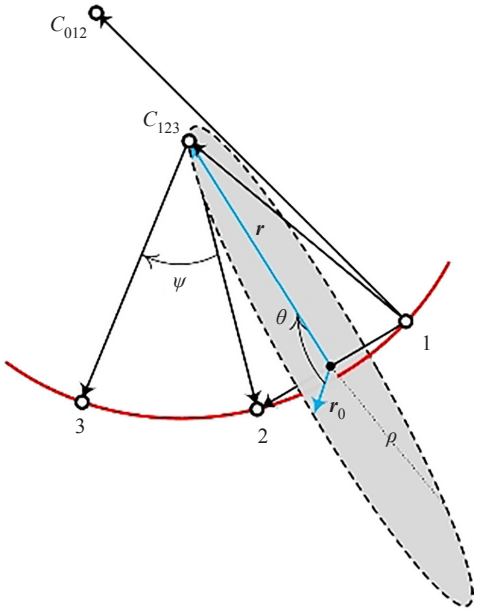

Figure 6. Geometrical Calculation of Point 3 from Points 1 and 2

Note that the argument (τ) is omitted in the equations for the sake of simplicity. To obtain C_{123}, we should rotate the vector $\boldsymbol{r_0}$ about the unit vector $\boldsymbol{u_1}$ by the angle θ. Rodriguez rotation formula may be used to obtain vector $\boldsymbol{r}$ in the global frame [50];

$$\boldsymbol{u_1} = \frac{\boldsymbol{r}_{1,2}}{|\boldsymbol{r}_{1,2}|}, \tag{14}$$

$$\tilde{\boldsymbol{u}}_{\boldsymbol{1}} = \begin{bmatrix} 0 & -u_{13} & u_{12} \\ u_{13} & 0 & -u_{11} \\ -u_{12} & u_{11} & 0 \end{bmatrix}, \tag{15}$$

$$R_{u_{1,\theta}} = \boldsymbol{I}cos\theta + \boldsymbol{u_1 u_1^T}(1-cos\theta) + \tilde{\boldsymbol{u}}_{\boldsymbol{1}} sin\theta, \tag{16}$$

$$\boldsymbol{r} = R_{u_{1,\theta}} \boldsymbol{r_0}, \tag{17}$$

where $\boldsymbol{u_1}$ is the unit vector along the rotation axis, $R_{u_{1,\theta}}$ is the rotation matrix, and the coordinates of the middle point between points 1 and 2 are obtained from $\frac{\boldsymbol{r_1}+\boldsymbol{r_2}}{2}$.

Having the size and orientation of the drawing circle defined, one may obtain the next point (point 3) on the curve in the global frame by using the Rodriguez formula once more, this time rotating $\boldsymbol{r}_{C_{123},2}$ by the angle ψ about the unit vector $\boldsymbol{u_2}$ (Figure 6);

$$\boldsymbol{u_2} = \frac{\boldsymbol{r}_{1,2} \times \boldsymbol{r}_{1,C_{123}}}{|\boldsymbol{r}_{1,2} \times \boldsymbol{r}_{1,C_{123}}|}, \tag{18}$$

$$\tilde{\boldsymbol{u}}_{\boldsymbol{2}} = \begin{bmatrix} 0 & -u_{23} & u_{22} \\ u_{23} & 0 & -u_{21} \\ -u_{22} & u_{21} & 0 \end{bmatrix}, \tag{19}$$

$$R_{u_{2,\psi}} = \boldsymbol{I}cos\psi + \boldsymbol{u}_{\boldsymbol{2}}\boldsymbol{u}_{\boldsymbol{2}}^{\boldsymbol{T}}(1-cos\psi) + \tilde{\boldsymbol{u}}_{\boldsymbol{2}}sin\psi, \tag{20}$$

$$\boldsymbol{r}_{C_{123},3} = R_{u_{2,\psi}}\boldsymbol{r}_{C_{123},2}. \tag{21}$$

Note that angle ψ represents the proceeding step of the curve generation and holds the same value between points 1-2 and 2-3. Therefore, according to the definition of dot product of vectors $\boldsymbol{r}_{1,C_{123}}$ and $\boldsymbol{r}_{C_{123},2}$, it may be calculated as;

$$\psi = \cos^{-1}\left(\frac{-\boldsymbol{r}_{1,C_{123}} \cdot \boldsymbol{r}_{C_{123},2}}{|\boldsymbol{r}_{1,C_{123}}||\boldsymbol{r}_{C_{123},2}|}\right). \tag{22}$$

Similarly, the next point (point 4) could be calculated using points 2 and 3 and so on. It is important to note that an upper and/or lower limit on the value of ψ may be imposed to have more control on the increments (i.e. road centerline resolution), without the loss of generality.

Note that we have not yet provided any information on the road bank angle $\gamma(\tau)$. This angle may be independently imposed on the road profile to complete its mathematical definition. In an alternative approach, one may define two separate curves and connect the corresponding points together to create a bank angle; such an approach may complicate the process and impose more restrictive constraints.

3.3.2 *Constraints and limits*

It is worth emphasizing that in terms of the road geometry, the location of the center of curvature only affects the longitudinal slope of the road; in other words, the lateral slope (bank angle) is inherently independent of the center of curvature. However, for the purpose of making the road safer and more comfortable for the drivers/passengers of turning vehicles, a certain bank angle as a function of the road curvature may be introduced by the designer. First, let us introduce the required limitation on the longitudinal slope of the road. Typical flat urban roads normally have a slope of less than ±10% [45], which may be written mathematically as;

$$-\tan^{-1}0.1 \le \phi \le \tan^{-1}0.1. \tag{23}$$

In terms of the variables depicted in Figure 6, the angle ϕ is obtained as;

$$\phi_{12} = \sin^{-1}\frac{Z_2 - Z_1}{|\boldsymbol{r}_{1,2}|}. \tag{24}$$

Although some limitations on the angle θ may be imposed to avoid excessively large slopes, this limitation on the slope is imposed on the resulting road geometry through a post-processing step in order to avoid unnecessary discontinuities in the location of the center of curvature. To realize this, after compilation of the whole road geometry, the maximum generated slope is measured and the whole sequence of road coordinates are vertically compressed (flattened), if necessary, to abide by the maximum allowable slope. This flattening is done by multiplying the z-coordinates of the points by the ratio of maximum allowable slope to the current observed maximum. It is worth mentioning that such a flattening will slightly distort the geometry from the initially intended one, but the consequences

are easily manageable, as discussed in the following sections.

Furthermore, because of the discrete nature of path generation in the proposed method, in order for the algorithm to be capable of changing the direction of turns, the allowable variation in θ denoted by $\Delta\theta$ must be a monotonically increasing function of the radius of curvature. In other words, if the road is highly curved, i.e. the radius of curvature is small, the variation in the location of center of curvature must be small to satisfy curvature continuity. On the other hand, when the road is close to a straight line, i.e. a very large radius of curvature, the variation in the center of curvature may be very large so that it even completely changes the direction of rotation, without causing any continuity issue. The following expression is used to relate the allowable variation in θ in each step;

$$-\frac{\pi}{180}(1+k(\rho-68)^E) \le \Delta\theta \le \frac{\pi}{180}(1+k(\rho-68)^E). \tag{25}$$

As for the constraints on the radius of curvature, let us consider two extreme cases; first, assuming the center of curvature to be on the horizontal plane, the limit of achievable lateral acceleration for a vehicle may be estimated as;

$$a_y = \frac{v^2}{\rho} < \mu g. \tag{26}$$

Therefore, there is a minimum achievable radius of curvature;

$$\rho > \frac{v^2}{\mu g}. \tag{27}$$

The other extreme condition for ρ appears when considering driving over a hill, where the center of curvature is located vertically below the vehicle. In this case, the only existing force that can provide the required centripetal acceleration is the gravity. Similarly, one may write;

$$a_z = \frac{v^2}{\rho} < g \rightarrow \rho > \frac{v^2}{g}. \tag{28}$$

Which is less limiting compared to a_y, due to the typical range of friction coefficient as $\mu < 1$. The conditions for combined vertical and lateral accelerations sit in between the above two extreme cases, therefore taking the lateral acceleration limit as the worst-case scenario guarantees that the vehicle will remain within the physically achievable limits of accelerations.

Taking the maximum design speed for the vehicle as $v_{max} = 20$ m/s and minimum friction coefficient of $\mu_{min} = 0.6$ for a wet road, the constraint on the radius of curvature becomes;

$$\rho > \frac{20^2}{(0.6)(9.81)} = 68m. \tag{29}$$

Furthermore, a maximum radius may be defined, indicating an upper limit on the radius of curvature above which the road may be deemed as a straight line. Here, a maximum of $\rho = 1000$ m is assumed for this purpose. Thus, $\Delta\rho$ will be adjusted in each step according to the current value of ρ.

It is important to note that the flattening process explained above for maintaining the required slopes may result in some segments of the road having unrealistically small radii of curvature after post-processing. This is because the segments of the road with too steep slopes may become highly curved sections, when the flattening occurs. However, this can be easily compensated by multiplying the x, y and z coordinates of the road waypoints with the proper

multiplier to scale up the whole road profile, if necessary. This way, although the continuity of the road and its curvature is maintained, a random entity is also introduced in the scale of the resulting geometry, making it less predictable, but in a controlled manner. Note that the final radius of curvature can be simply obtained using the radius of the circumscribed circle of the triangle constructed by each set of three consecutive waypoints with a, b and c denoting the sides of that triangle and $s = \frac{a+b+c}{2}$ [51];

$$\rho' > \frac{abc}{4\sqrt{s(s-a)(s-b)(s-c)}}. \tag{30}$$

In addition to the scaling mentioned above, it is also advisable to define a threshold for maximum slope before accepting a certain resulting road geometry as an eligible one to be flattened; this way, the cases requiring too much flattening will be automatically discarded, eliminating the outliers.

3.3.3 *Bank angle calculation*

Normally, the road bank angle is calculated based on the principle that the vehicle would not need any steering action from the driver at the design speed to remain on the track. In other words, the required lateral force is generated through the vertical reaction forces under the tires [52]. In case of a 3D road geometry, the center of curvature may be located above/below the horizontal surface, creating a situation shown in Figure 7, assuming the mass center is on the road centerline.

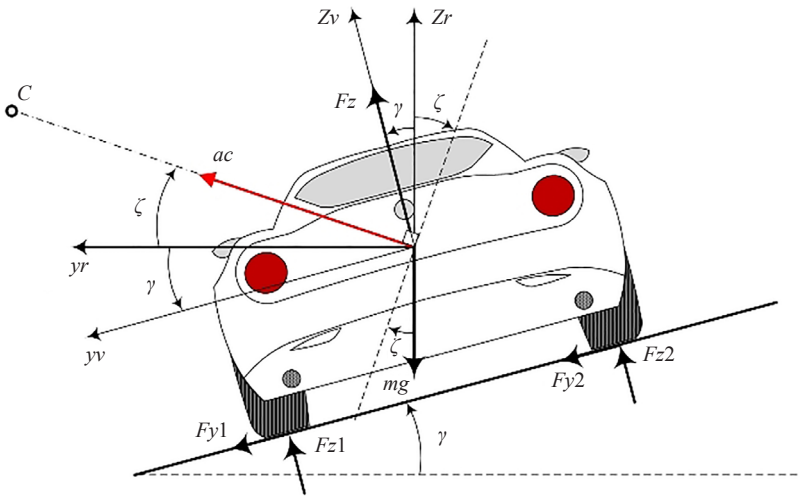

Figure 7. A turning vehicle on a road with a bank angle

In such a situation, for the bank angle to completely eliminate lateral tire force requirements, equations of motion along and perpendicular to the centripetal acceleration vector are;

$$F_z \cos(\zeta + \gamma) = mg \cos\zeta, \tag{31}$$

$$F_z \sin(\zeta + \gamma) = mg \sin\zeta + m\frac{v^2}{\rho}, \tag{32}$$

which yields;

$$\gamma = \tan^{-1}\left(\tan\zeta + \frac{v^2}{\rho g \cos\zeta}\right) - \zeta. \tag{33}$$

This ultimate bank angle in the general case follows the surface plot of Figure 8, according to the values of ρ and ζ.

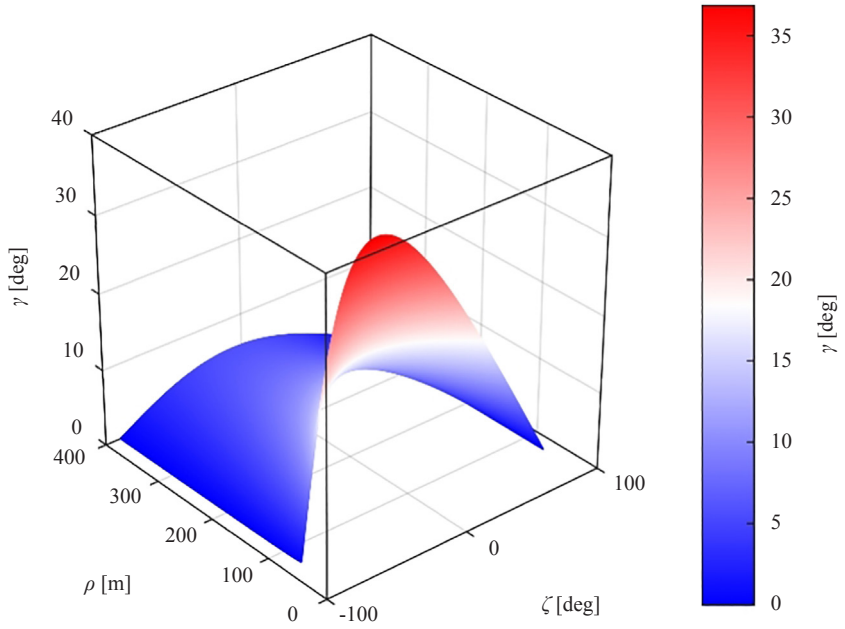

Figure 8. Unconstrained bank angle calculation in a general case

However, for realistic road design which also takes into account the passenger comfort, a threshold for acceptable bank angle needs to be defined. A typical bank angle observed at a regular design speed for highways may be designated as the maximum allowable bank angle. Consider a turning section of a road in the horizontal plane $\zeta = 0$. For a regularly experienced lateral acceleration of $\frac{v^2}{\rho} = 0.75$ m/s^2 =0.08 g [53], using (33) the required bank angle becomes;

$$\gamma_{\max} = \tan^{-1}\frac{v^2}{\rho g} = \tan^{-1} 0.08 \approx 4.5\,\text{deg}, \tag{34}$$

$$\gamma(\tau) = \text{sat}\left[\tan^{-1}(\tan\zeta + \frac{v^2}{\rho g \cos\zeta}) - \zeta,\ \gamma_{\max}\right], \tag{35}$$

where sat(x, L) is the saturation function and defined as;

$$\text{sat}(x, L) = \begin{cases} L & x > L \\ x & -L \le x \le L \\ -L & x < -L \end{cases}, \tag{36}$$

Note that the final bank angle in equation (34) uses the saturation function as described in (35) to choose between the theoretical bank angle in (32) or the maximum allowable bank angle in (33); therefore not allowing the banking angle to grow excessively large. The design speed of the road is set to $v = 20$ m/s, and the angle $\zeta(\tau)$ is obtained from the location of center of rotation relative to the road as;

$$\zeta(\tau) = \text{atan2}\left[\frac{r_3(\tau)}{\rho(\tau)},\ \frac{\hat{j}_r \cdot \boldsymbol{r}(\tau)}{\rho(\tau)}\right], \tag{37}$$

where r_3 is the z-coordinate of the road at point τ, and the unit vectors of the road coordinate frame are;

$$\hat{i}_r = \frac{\boldsymbol{r}_{i,i+1}}{|\boldsymbol{r}_{i,i+1}|}, \tag{38}$$

$$\hat{k}_r = \hat{K}, \tag{39}$$

$$\hat{j}_r = \hat{k}_r \times i_r. \tag{40}$$

3.4 *Chaotic data acquisition and implementation*

An entirely numerical approach has been chosen to derive the datasets for the road generation algorithm. This is primarily due to the need for many datasets with optional variations in the signal's time steps that were critical to the proper behavior of random number generation. Otherwise, extracting data from an electronically built circuit would be impractical in our case. As the first step, the system of differential equations denoting Chua's circuit has been solved numerically by Livermore Solver for Ordinary Differential Equations (LSODE) algorithm. Then, in order to achieve a somewhat uniform distribution within the dataset, different time steps were evaluated for reading chaotic data, which was later incorporated into the main algorithm for generating roads.

In the aforementioned geometrical approach, there are certain parameters that have a critical impact on the random nature of the generated road profile. Rotation angle θ and radius ρ are obtained indirectly from the chaotic data of the numerically solved Chua's circuit equations. By considering a typical road and tire compound on dry asphalt, the maximum allowable curvature of the road is obtained. Thus, the limitated boundaries of the radius are allocated. As the next step, after normalizing the chaotic signal, a dataset featuring acceptable radius values which are practically random is obtained. The dataset for parameter θ went through the same approach with differences in the acceptable range of the rotation angle. For having a rather smoother curve for the road, several time steps for extracting the chaotic data experimented as trial-and-error attempts, and the value $t = 0.37$ s was considered as the fittest value.

To illustrate the road generating algorithm, simplified pseudocode is represented as below. The algorithm starts with randomly initializing of the first two points on the curvature namely P_1 and P_2, and an additional necessary point for locating the center of a circle in the first iteration namely C_{012}. Initialized variables are mostly calculated by trial and error to provide an acceptable realistic road profile. the algorithm then calculates the values of theta and rho for each iteration based on their initialized values and configured limitations which are discussed in detail in sub-section 3.3.1. Other parameters are computed as well, with respect to the stated formulae in sub-section 3.3, until the next point on curvature is reached in every iteration. It is necessary to limit ϕ_{23}, indicating the slope of the curvature, so that it falls inside the appropriate boundary that prevents our algorithm to result in an unrealistic road profile with sudden or extreme jumps in the slope of the generated road. The limitation is applied by a flattening method using the *kz* variable. Also, the banking angle is calculated at the last level as an extra evaluation parameter of the generated curvature. These steps take place for each ρ and θ, and the sequence of obtained points forms the road 3D curve eventually.

	Block algorithm for road generating using chaotic data
1	**INPUTS:** *ρ-series*, *θ-series*
2	**OUTPUTS:** *road-coordinates*
3	**INIT** P_1, P_2, C_{012} (randomly)
4	**INIT** ρ_{max} with 1000
5	**SET** $\rho = \rho_{max}$
6	**INIT** θ with $\pi/2$
7	**INIT** ψ with $\lvert p_2 - p_1 \rvert / \rho$
8	**INIT** ϕ with asin $(p_1 \times z - p_2 \times z) / \lvert p_2 - p_1 \rvert$
9	**INIT** $d\theta$ with 0
10	**INIT** $d\rho$ = avg (10 * (2 * *ρ-series*)) with kernel size 100
11	**FOR** *i* **FROM** 1 **TO** size(*ρ-series*)
12	**SET** ρ = min (ρ_{max} , max (68 , $r + d\rho[i]$))
13	**SET** $k = 90/(\rho_{max} - 68)$ ^ 40
14	**SET** $d\theta = \pi/180$ * (1 + k * (ρ - 68) ^ b) * (2 * *θ-series*[*i*])
15	**SET** θ = mod ($\pi/2 + d\theta$, 2 * π)
16	**COMPUTE** r_0 using eq. 13
17	**COMPUTE** u_1 using eq. 14
18	**SET** $\tilde{u}_1$ = [[0, -u_1[2], u_1[1]] = [u_1[2], 0, -u_1[0]] = [-u_1[1], u_1[0], 0]]
19	**COMPUTE** $R_{u_1, \theta}$ using eq. 16
20	**COMPUTE** r using eq. 17
21	**LOCATE** C_{123}
22	**COMPUTE** ψ using eq. 22
23	**SET** ψ = max(ψ, π/180 * 0.01)
24	**COMPUTE** u_2 using eq. 18
25	**SET** $\tilde{u}_2$ = [[0, -u_2[2], u_2[1]] = [u_2[2], 0, -u_2[0]] = [-u_2[1], u_2[0], 0]]
26	**COMPUTE** $R_{u_2, \psi}$ using eq. 20
27	**COMPUTE** $r_{C_{123}, 3}$ using eq. 21
28	**LOCATE** P_3
29	**APPEND** C_{123} to *centers*
30	**APPEND** p_3 to *road-coordinates*
31	**COMPUTE** $\phi 23$ using eq. 24
32	**APPEND** $\phi 23$ to ϕ
33	**END FOR**
34	**SET** kz = min(1, tan(0.1)/max(|tan(ϕ)|))
35	**SET** ϕ = atan(tan(ϕ) * kz)
36	**SET** *road-coordinates*.z = *raod-coordinates*.z * kz
37	**PLOT** *road-coordinates*
38	**COMPUTE** $\gamma(\tau)$ using eq. 35

3.5 *Hypothetical results and evaluation criteria*

To ensure the resulting road profile is feasible in terms of vehicle dynamics and tire-road friction considerations, a Tire Friction Usage (TFU) function is defined in this section, which will be calculated along the generated path to evaluate its consistency with vehicle dynamics. The TFU is defined as the ratio of current friction force to maximum tire force capacity according to the vertical tire load, assuming a linear relationship between the available tire friction and the vertical load. Any value of TFU less than unity is considered feasible, while the values larger than unity indicate conditions beyond the handling capacity of the vehicle. Referring back to Figure 7, the vertical force F_z may be calculated by considering equilibrium along z_v axis;

$$F_z = m\left[g\cos\gamma + \frac{v^2}{\rho}\cos(\frac{\pi}{2} - \gamma - \zeta)\right] = m\left[g\cos\gamma + \frac{v^2}{\rho}\sin(\gamma + \zeta)\right]. \tag{41}$$

The maximum achievable friction force, assuming the minimum value of friction coefficient to represent a wet surface, becomes;

$$F_{\max} = \mu_{\min} F_z. \tag{42}$$

Although certain bank angles $\gamma(\tau)$ are introduced, portions of the lateral force may still be required to be generated through lateral tire friction forces. Along the lateral vehicle axis y_v, one may write;

$$F_y = ma_C\cos(\gamma + \zeta) - mg\sin\gamma = m\frac{v^2}{\rho}\cos(\gamma + \zeta) - mg\sin\gamma. \tag{43}$$

Therefore;

$$TFU = \frac{F_y}{F_{\max}} = \frac{\frac{v^2}{\rho}\cos(\gamma + \zeta) - g\sin\gamma}{\mu_{\min}\left[g\cos\gamma + \frac{v^2}{\rho}\sin(\gamma + \zeta)\right]}. \tag{44}$$

4. Results and discussion

A vivid illustration of the alteration patterns in the chaotic signal of Chua's circuit, after being converted to the range between 0-1, is presented in Figure 9. In compliance with the upcoming sections of the representation of the results, Figure 9 illustrates 20 samples of the chaotic signal. As the chaotic/random nature of the core signal allows, there is no inherent distinction between re-running the numerical data acquisition process or starting the sampling process simply from different starting points in a rather longer signal. The latter has been opted for the generation of the signals illustrated in Figure 9, and later implementation in the road generation algorithm. It is to witness, that not only the data points along each sequence show scattered, random (seemingly) behavior, but each sequence also shows excessive individuality in comparison with the other signals in the set.

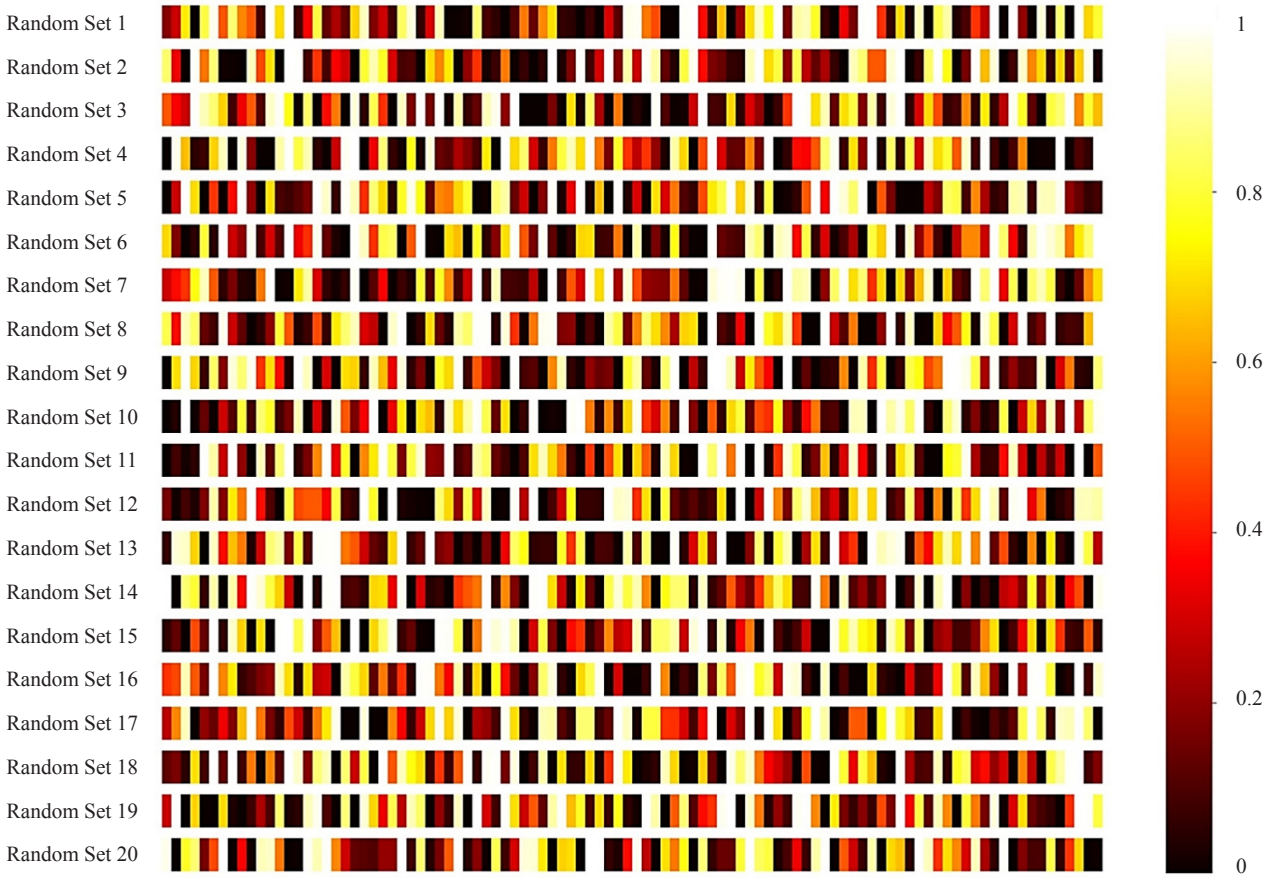

Figure 9. Heatmap of chaotic data converted to the range between 0 and 1

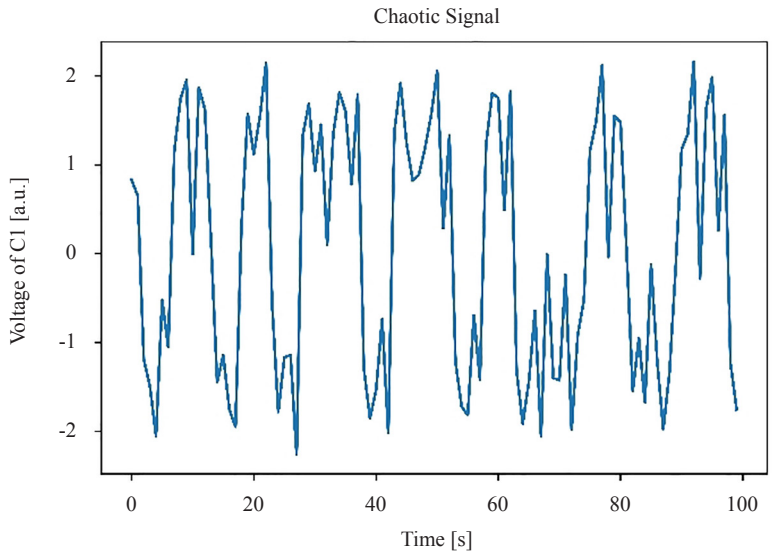

Figure 10. Chaotic signal of capacitor 1 in Chua's circuit

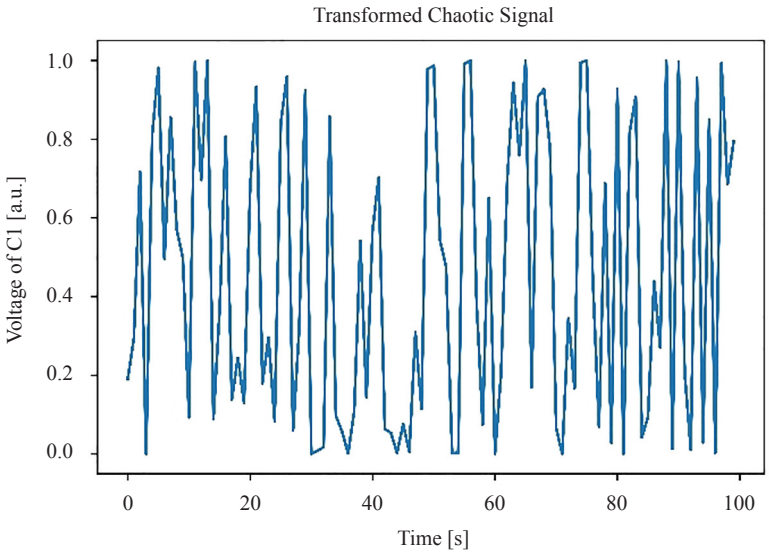

Figure 11. Converted signal of capacitor 1 in Chua's circuit between 0-1

In Figure 10, the raw data derived from Chua's circuit equations are observed. For applying the random sequence to the main algorithm of the road generation, its range should have been converted to [0, 1]. For this purpose, a two-step conversion was designed. First, the signal was converted to [0, 2π], then the data were inserted into the sin function to have the arbitrary range of [0, 1] (Figure 11).

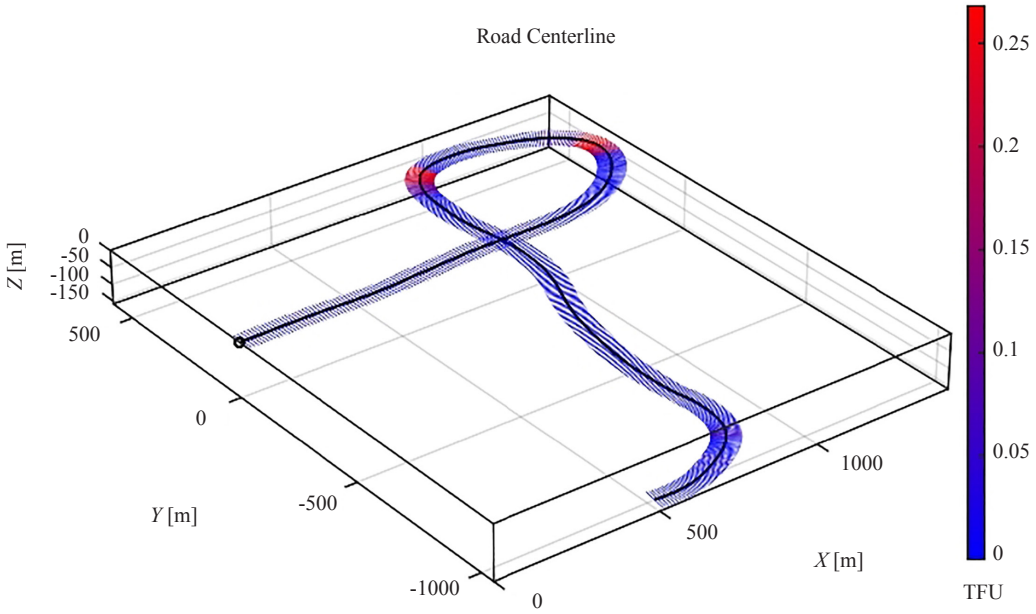

Figure 12. A sample road generated using 30,000 waypoints

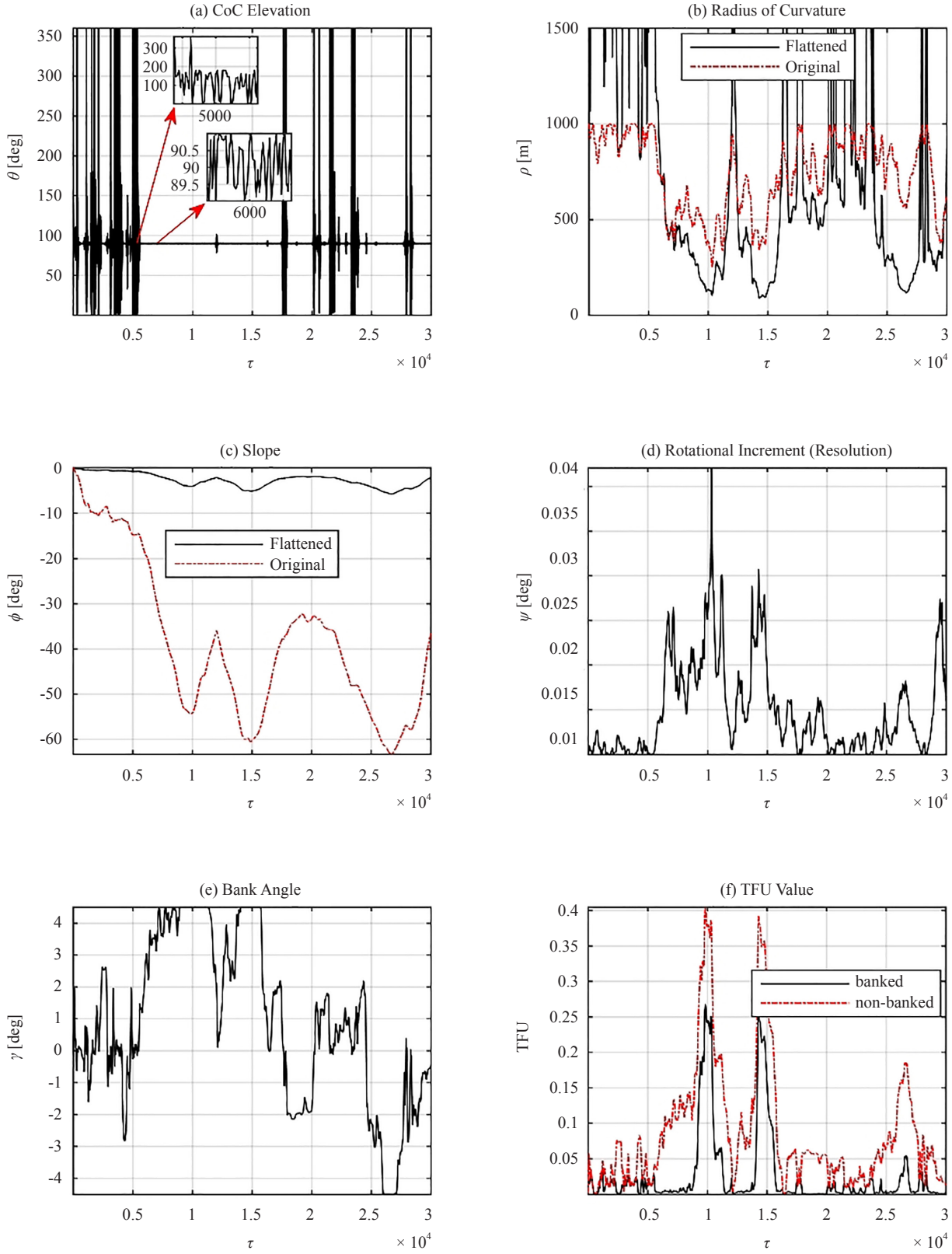

Figure 13. Parameters of the generated sample road; a) CoC elevation, b) radius of curvature, c) slope, d) rotational increment (resolution), e) bank angle, f) TFU value

To present and analyze the resulting road geometries, the proposed road generation algorithm is applied to a fixed number of waypoints. Figure 12 shows a sample road generated using 30,000 waypoints (resolution). The transversal lines along the road centerline are schematic indicators of the bank angles and the road surface. The color spectrum along the road also indicates the values of TFU, and shows the amount of used tire force capacity to negotiate each segment of the road. As indicated in the figure with a circle, the road starts at (0, 0, 0), and the waypoints are produced step-by-step to construct the centerline. The banking of the road is also constructed following the procedure explained in the previous section, with consideration of smoothening the variations in the bank angle, as it is not a hard constraint to be met, but rather a helpful feature to minimize the tire usage. It is evident from the figure that the most difficult segments of the road, in terms of tire force requirement, are associated with large curvatures or a relatively sudden decrease of the slope, as expected. The figure shows a clear example of how the slopes and curvatures may vary along the path, by producing both left and right turns, as intended. The length of the road in this sample is around 3500m.

Figure 13-a shows the variations of θ associated with this sample output, respectively. Note that although the variations in θ seem abrupt and have high frequencies, this does not negatively affect the curvature continuity of the road due to two reasons: 1-the magnified subplots indicate the continuous variations of θ around two sample points on the figure, showing reasonable continuity between adjacent waypoints; 2-the amplitude of variations is controlled using (29), which allows the CoC to turn considerably more, when the radius of curvature is large (see the magnified plot around point 5000), resulting in microscopic changes of direction for the incremental road segments to be compared with very small variations in the CoC, when the radius of curvature is small (see the magnified plot around point 6000).

Figure 13-b demonstrates the variations in the radius of curvature ρ, both for the originally generated values and after the flattening process. The original radius is limited between the minimum and maximum set values. However, the potential flattening, which was necessary in this sample to ensure the slopes fit in the desired limit, cause distortion in the range of radii of curvature along the path, as explained in the previous sections. The flattened radii are still reasonably smooth in variations, especially at small radii. It is worth mentioning, that although larger variations with higher frequencies are observed in radii of larger than 1000 m, such variations are considered reasonable and do not cause curvature discontinuity in the path, because they refer to considerably large radii of curvature, similar to the discussion on θ variations.

Figure 13-c demonstrates the slope along the road, both for original and flattened cases. It can be seen that the original slope was well-beyond the set limit of around 5.7 deg. However, the fattening process has forced the slopes to remain within the boundaries of the allowable values. Figures 13-d and 13-e demonstrate the rotational increment angle ψ, and the bank angle γ, respectively. An applied lower limit of 0.01 deg on the angle ψ is evident in the figure. The banking of the road is also shown to be limited by the upper limit of 4.5 deg, as intended.

The TFU values are plotted in Figure 13-f, indicating that the resulted road is completely feasible to be tracked by a vehicle, by having TFU values of less than 1.0 along the road. Note that the non-banked curve is included to compare the effect of introducing banking as per (35), with a road that does not feature any banking. It can be seen that although the non-banked case also satisfies the feasibility conditions, introducing banking generally reduces the tire usage ratio as well as expanding the safety margin throughout the turns.

Figure 14 illustrates the TFU values of the same road if it was to be negotiated with three different velocities of 20, 25, and 30 m/s. Note that the road is designed to be compatible with a maximum velocity of 20 m/s. However, it can be seen that even traveling at 25 m/s is feasible as the peak TFU value is just below 1.0, demonstrating a slightly conservative design. This is due to the fact that the minimum radius of curvature was calculated with a worst-case scenario assumption, that the CoC is on the horizontal plane; however, the actual curvature can be thought of having both horizontal and vertical components, therefore not necessarily imposing such big risks of lack of lateral tire force. Nevertheless, the speed of 30 m/s has peak TFU values much larger than 1 (vertical axis range is limited for the sake of enabling visual comparison), therefore infeasible. Furthermore, it is worth noting that the TFU value does not increase in proportion to speed, because the vertical tire forces become smaller when the vehicle passes through peaks of the hills, causing the denominator of the TFU (i.e. the maximum achievable lateral force) to approach zero. Consequently, the vehicle gets close to losing tire-road contact and becomes uncontrollable.

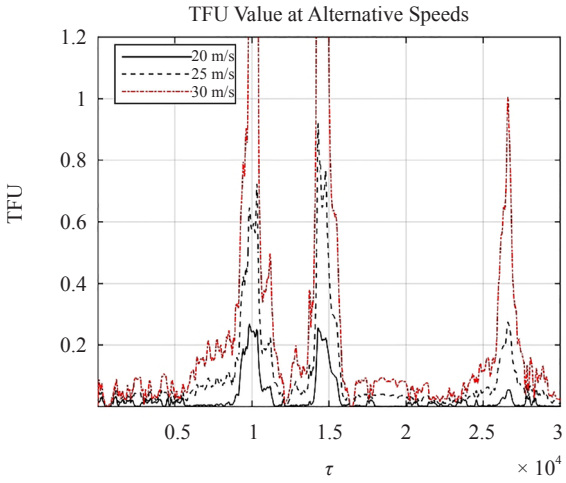

Figure 14. Hypothetical TFU values at different speeds

Several resulting road geometries with 30,000 waypoints are depicted in Figure 15. All the roads are generated using iterations of the same algorithm with no alteration of design parameters. The figure indicates the diversity of the resulting road geometries through a wide variety of different curvatures, slopes, and even road lengths, which are affected by the random nature of the road generation algorithm.

5. Conclusions

A stochastic random road generation algorithm was developed and introduced, which uses properly generated random number sequences to construct a physically meaningful complex three-dimensional road geometry to be used in future studies requiring simulated versatile road shapes. The proposed method is able to produce realistic curvature and slope properties and was also equipped with a banking geometry, making it more suitable for the vehicles to track. The proposed process can be done in an offline setting, where a virtual environment is required to be developed prior to simulating the motion of the vehicle for vehicle control, stability, energy management, or any other particular investigation.

It is worth noting, that the proposed method is a novel fundamental approach towards road modeling; therefore, its scope is limited to only include the most important aspect of the vehicle environment, namely the road geometry, and is able to generate a complex three-dimensional road geometry. However, the proposed method is expandable, and it may be complemented with additional information, such as the road signage data, speed limits, city traffic scenarios, driving cycles, road roughness data, etc. to represent a more comprehensive simulation environment for evaluation and testing.

A comprehensive function describing the feasibility level of the generated road is introduced, which compares the required tire friction with the maximum available friction based on the vertical tire forces and the road geometry in three-dimensional space. The outputs of the road generation algorithm show promising results both in terms of feasibility of the road segments and versatility of the produced geometries, which are crucial for training AI-based controllers. The results also demonstrate complete consistency with road design principles, including the slope and curvature limit and continuity.

It was shown that the proposed method is capable of producing random roads with predefined constraints. Based on the design principles and the requirements of each individual application, the user may decide on the parameters involved and then allow the algorithm to generate the outputs in a huge number of iterations, eliminating the need for manually producing such complex geometries and increasing the fidelity of the study by removing operator bias. Therefore, the proposed methodology contributes to the field of applied mathematics and vehicle dynamics by introducing a mathematical approach for developing a physically meaningful geometry, representing real-life situations, and facilitating the evaluation of vehicle and traffic control systems in simulations.

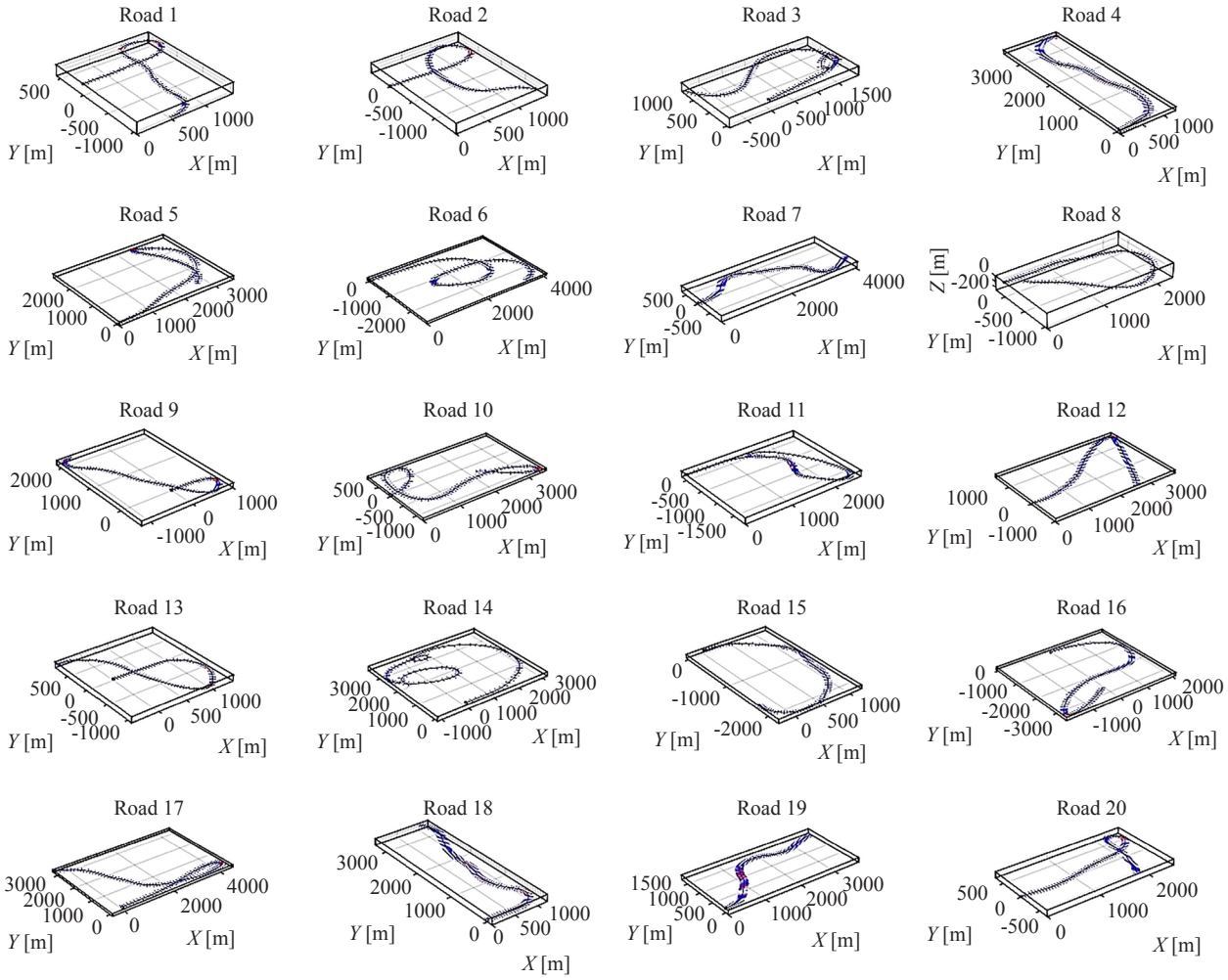

Figure 15. Samples of the resulting random road geometries

Conflict of interest

The authors declare that there is no personal or organizational conflict of interest with this work.

References

[1] Tsonis AA. *Chaos from theory to applications*. 1st ed. Springer Science and Business Media New York; 1992.

[2] Strogatz SH. *Nonlinear dynamics and chaos: With applications to physics, biology, chemistry and engineering*. Westview Press; 2000.

[3] Barrow-Green J. *Poincaré and the three body problem*. American Mathematical Society/London Mathematical Society; 1997.

[4] Lorenz EN. Deterministic nonperiodic flow. *Journal of the Atmospheric Sciences*. 1963; 20: 130.

[5] Pecora LM, Carroll TL. Synchronization in chaotic systems. *Physical Review Letters*. 1990; 64: 821-824.

[6] Callegari S, Rovatti R, Setti G. Embeddable ADC-based true random number generator for cryptographic applications exploiting nonlinear signal processing and chaos. *IEEE Trans Signal Process*. 2005; 53(2): 793-805. Available from: http://dblp.uni-trier.de/db/journals/tsp/tsp53.html#CallegariRS05.

[7] Zhao L, Liao X, Xiao D, Xiang T, Zhou Q, Duan S. True random number generation from mobile telephone photo based on chaotic cryptography. *Chaos, Solitons & Fractals*. 2009; 42(3): 1692-1699. Available from: https://doi.

org/10.1016/j.chaos.2009.03.068.
[8] Stipcevic M, Koç ÇK. True random number generators. In: Koç Ç. (ed.) *Open Problems in Mathematics and Computational Science*. 2014. p. 275-315. Available from: http://dblp.uni-trier.de/db/books/collections/K2014.html#StipcevicK14.
[9] Momtaz A, Qoreishi E, Amini S, Khayami H, Amini K, Haddadian S. Generation of a pseudo random number sequence by implementation of mathematically manipulated chaotic signals of quasi-synchronized chua's circuits equations, for symmetric encryption purposes. *Information Security and Applications*. Elsevier; 2021.
[10] Amini K, Momtaz A, Qoreishi E, Amini S, Haddadian S. Monte carlo approach towards evaluating random number generators based on mathematical schemes driven from chua's circuit. *Journal of Contemporary Mathematics*. 2020; 1(4): 253-271. Available from: https://doi.org/10.37256/cm.142020491.
[11] Amini K., Momtaz A., Qoreishi E., Amini S., Haddadian S. On the evaluation criteria for random number generators using monte carlo integration algorithm. *Current Topics on Mathematics and Computer Science*. 2021; 3: 126-150. Available from: https://doi.org/10.9734/bpi/ctmcs/v3/10247D.
[12] Datcu O, Macovei C, Hobincu R. Chaos based cryptographic pseudo-random number generator template with dynamic state change. *Applied Sciences*. 2020; 10(2): 451. Available from: http://dx.doi.org/10.3390/app10020451.
[13] Lynnyk V, Sakamoto N, Celikovsky S. Pseudo random number generator based on the generalized Lorenz chaotic system. *IFAC-PapersOnLine*. 2015; 48(18): 257-261. Available from: https://doi.org/10.1016/j.ifacol.2015.11.046.
[14] Rezk AA, Madian AH, Radwan AG, Soliman AM. Reconfigurable chaotic pseudo random number generator based on FPGA. *AEU-International Journal of Electronics and Communications*. 2019; 94: 174-180. Available from: https://doi.org/10.1016/j.aeue.2018.10.024.
[15] Karakaya B, Gülten A, Frasca M. A true random bit generator based on a memristive chaotic circuit: Analysis, design and FPGA implementation. *Chaos, Solitons & Fractals*. 2019; 119: 143-149. Available from: https://doi.org/10.1016/j.chaos.2018.12.021.
[16] Milos D, Pavol G. Chaos-based true random number generator embedded in a mixed-signal reconfigurable hardware. *Journal of Electrical Engineering*. 2006; 57: 218-225.
[17] Ergün S, Tanrıseven S. Random number generation using dual oscillator architecture and discrete-time chaos. *2018 International Symposium on Electronics and Smart Devices (ISESD)*. IEEE; 2018. p. 1-4. Available from: https://doi.org/10.1109/ISESD.2018.8605452.
[18] Dhanuskodi SN, Vijayakumar A, Kundu S. A chaotic ring oscillator based random number generator. *2014 IEEE International Symposium on Hardware-Oriented Security and Trust (HOST)*. IEEE; 2014. p. 160-165. Available from: https://ieeexplore.ieee.org/document/6855588/.
[19] Rouillard V, Sek MA, Bruscella B. Simulation of road surface profiles. *Journal of Transportation Engineering*. 2001; 127(3): 247-253. Available from: https://doi.org/10.1061/(ASCE)0733-947X(2001)127:3(247).
[20] Rustighi E, Elliott SJ. Stochastic road excitation and control feasibility in a 2D linear tyre model. *Journal of Sound and Vibration*. 2007; 300(3-5): 490-501. Available from: https://doi.org/10.1016/j.jsv.2006.06.076.
[21] Yonglin Z, Jiafan Z. Numerical simulation of stochastic road process using white noise filtration. *Mechanical Systems and Signal Processing*. 2006; 20(2): 363-372. Available from: https://doi.org/10.1016/j.ymssp.2005.01.009.
[22] Feng J, Zhang X, Guo K, Ma F, Karimi HR. A frequency compensation algorithm of four-wheel coherence random road. *Mathematical Problems in Engineering*. 2013; 2013. Available from: https://doi.org/10.1155/2013/986584.
[23] Sheng KY, Abdullah S, Haris SM, Omar MZ, Schramm D. Generation of artificial road profile for automobile spring durability analysis. *Jurnal Kejuruteraan*. 2018; 30(2): 123-128. Available from: http://dx.doi.org/10.17576/jkukm-2018-30(2).
[24] Dharankar CS, Hada MK, Chandel S. Numerical generation of road profile through spectral description for simulation of vehicle suspension. *Journal of the Brazilian Society of Mechanical Sciences and Engineering*. 2017; 39: 1957-1967. Available from: https://doi.org/10.1007/s40430-016-0615-6.
[25] Schiehlen W. White noise excitation of road vehicle structures. *Sadhana*. 2006; 31: 487-503.
[26] Jiang CD, Cheng L, Fengchun S, Hongjie C. Simulation of road roughness based on using IFFT method. *2012 Third World Congress on Software Engineering*. IEEE; 2012. p. 190-193. Available from: https://doi.org/10.1109/WCSE.2012.46.
[27] Munari LA, Fontanella L, Hoss L, Marczak RJ. *Retrieving road surface profiles from PSDs for ride simulation of vehicles (No. 2012-36-0003)*. SAE Technical Paper. 2012. Available from: https://doi.org/10.4271/2012-36-0003.
[28] Robson JD, Dodds CJ. Stochastic road inputs and vehicle response. *Vehicle System Dynamics*. 1976; 5(1-2): 1-13.
[29] Robson JD, Kamash KM. Road surface description in relation to vehicle response. *Vehicle System Dynamics*. 1977; 6(2-3): 153-157.
[30] Dodds CJ, Robson JD. The description of road surface roughness. *Journal of Sound and Vibration*. 1973; 31(2):

175-183. Available from: https://doi.org/10.1016/S0022-460X(73)80373-6.
[31] Khosla D. Accurate estimation of forward path geometry using two-clothoid road model. *IEEE Intelligent Vehicle Symposium*. 2002; 1: 154-159. Available from: https://doi.org/10.1109/IVS.2002.1187944.
[32] Yagi Y, Brady M, Kawasaki Y, Yachida M. Active contour road model for smart vehicle. *Proceedings 15th International Conference on Pattern Recognition. ICPR-2000*. 2000; 3: 811-814. Available from: https://doi.org/10.1109/ICPR.2000.903668.
[33] Loose H, Franke U. B-spline-based road model for 3d lane recognition. *13th International IEEE Conference on Intelligent Transportation Systems*. IEEE; 2010. p. 91-98. Available from: https://doi.org/10.1109/ITSC.2010.5624968.
[34] Wang Y, Bai L, Fairhurst M. Robust road modeling and tracking using condensation. *IEEE Transactions on Intelligent Transportation Systems*. IEEE; 2008. p. 570-579. Available from: https://doi.org/10.1109/TITS.2008.2006733.
[35] Southall B, Taylor CJ. Stochastic road shape estimation. *Proceedings Eighth IEEE International Conference on Computer Vision, ICCV*. IEEE; 2001. p. 205-212. Available from: https://doi.org/10.1109/ICCV.2001.937519.
[36] Wang J, Lawson G, Shen Y. Automatic high-fidelity 3D road network modeling based on 2D GIS data. *Advances in Engineering Software*. 2014; 76: 86-98. Available from: https://doi.org/10.1016/j.advengsoft.2014.06.005.
[37] Wang H, Wu Y, Han X, Xu M, Chen W. Automatic generation of large-scale 3D road networks based on GIS data. *Computers & Graphics*. 2021; 96: 71-81. Available from: https://doi.org/10.1016/J.CAG.2021.02.004.
[38] Amara Y, Amamra A, Khemis S. Raw GIS to 3D road modeling for real-time traffic simulation. *The Visual Computer*. 2020; 1-18. Available from: https://doi.org/10.1007/s00371-020-02013-1.
[39] Huang W, Bevly DM, Schnick S, Li X. Using 3D road geometry to optimize heavy truck fuel efficiency. *IEEE 11th International IEEE Conference on Intelligent Transportation Systems*. IEEE; 2008. p. 334-339. Available from: https://doi.org/10.1109/ITSC.2008.4732656.
[40] Jo K, Sunwoo M. Generation of a precise roadway map for autonomous cars. *IEEE Transactions on Intelligent Transportation Systems*. 2013; 15(3): 925-937. Available from: https://doi.org/10.1109/TITS.2013.2291395.
[41] Mao Y, Li Y. An efficient method of 3D road automatic generating. *Proceedings of 2011 International Conference on Electronic & Mechanical Engineering and Information Technology IEEE*. IEEE; 2011. p. 4048-4051. Available from: https://doi.org/10.1109/EMEIT.2011.6023941.
[42] Zeng X, Wang J. A parallel hybrid electric vehicle energy management strategy using stochastic model predictive control with road grade preview. *IEEE Transactions on Control Systems Technology*. 2015; 23(6): 2416-2423. Available from: https://doi.org/10.1109/TCST.2015.2409235.
[43] Khayyam H. Stochastic models of road geometry and wind condition for vehicle energy management and control. *IEEE Transactions on Vehicular Technology*. 2012; 62(1): 61-68. Available from: https://doi.org/10.1109/TVT.2012.2218137.
[44] Johannesson P, Podgórski K, Rychlik I, Shariati N. AR (1) time series with autoregressive gamma variance for road topography modeling. *Probabilistic Engineering Mechanics*. 2016; 43: 106-116. Available from: https://doi.org/10.1016/j.probengmech.2015.12.006.
[45] Odrigo A, El-Gindy M, Pettersson P, Nedělková Z, Lindroth P, Öijer F. Design and development of a road profile generator. *International Journal of Vehicle Systems Modelling and Testing*. 2016; 111(3): 217-233. Available from: https://doi.org/10.1504/IJVSMT.2016.080875.
[46] Pettersson P. Operating cycle representations for road vehicles. PhD Thesis, Chalmers University of Technology, Sweden; 2019.
[47] Torabi S. Fuel efficient driving strategies. PhD Thesis, Chalmers University of Technology, Sweden; 2020.
[48] Chua LO. Chua's circuit: An overview ten years later. *Journal of Circuits, Systems and Computers*. 1994; 4(2): 117-159. Available from: https://doi.org/10.1142/S0218126694000090.
[49] Chua LO. Chua circuit. *Scholarpedia*. 2007; 2(10): 1488. Available from: http://dblp.uni-trier.de/db/journals/scholarpedia/scholarpedia2.html#Chua07.
[50] Jazar RN. *Advanced dynamics: Rigid body, multibody, and aerospace applications*. John Wiley & Sons; 2011.
[51] Holme A. *Geometry: Our cultural heritage*. Springer Science & Business Media; 2010.
[52] Jazar RN. *Vehicle dynamics: Theory and application*. Springer; 2017.
[53] Xu J, Yang K, Shao Y, Lu G. An experimental study on lateral acceleration of cars in different environments in Sichuan, Southwest China. *Discrete Dynamics in Nature and Society*. 2015; 2015. Available from: https://doi.org/10.1155/2015/494130.